Changes in Scleral Collagen Organization in Murine Chronic Experimental Glaucoma

Jacek K. Pijanka,[1] Elizabeth C. Kimball,[2] Mary E. Pease,[2] Ahmed Abass,[1] Thomas Sorensen,[3] Thao D. Nguyen,[4] Harry A. Quigley,[2] and Craig Boote[1]

[1]Structural Biophysics Group, School of Optometry and Vision Sciences, Cardiff University, Cardiff, United Kingdom
[2]Glaucoma Center of Excellence, Wilmer Ophthalmological Institute, Johns Hopkins University, Baltimore, Maryland, United States
[3]Diamond Light Source, Didcot, United Kingdom
[4]Department of Mechanical Engineering, Johns Hopkins University, Baltimore, Maryland, United States

PURPOSE. The organization of scleral collagen helps to determine the eye's biomechanical response to intraocular pressure (IOP), and may therefore be important in glaucoma. This study provides a quantitative assessment of changes in scleral collagen fibril organization in bead-induced murine experimental glaucoma.

METHODS. Wide-angle X-ray scattering was used to study the effect of bead-induced glaucoma on posterior scleral collagen organization in one eye of 12 CD1 mice, with untreated fellow eyes serving as controls. Three collagen parameters were measured: the local preferred fibril directions, the degree of collagen anisotropy, and the total fibrillar collagen content.

RESULTS. The mouse sclera featured a largely circumferential orientation of fibrillar collagen with respect to the optic nerve head canal. Localized alteration to fibril orientations was evident in the inferior peripapillary sclera of bead-treated eyes. Collagen anisotropy was significantly ($P < 0.05$) reduced in bead-treated eyes in the superior peripapillary (Treated: 43 ± 8%; Control: 49 ± 6%) and midposterior (Treated: 39 ± 4%; Control: 43 ± 4%) sclera, and in the peripapillary region overall (Treated: 43 ± 6%; Control: 47 ± 3%). No significant differences in total collagen content were found between groups.

CONCLUSIONS. Spatial changes in collagen fibril anisotropy occur in the posterior sclera of mice with bead-induced chronic IOP elevation and axonal damage. These results support the idea that dynamic changes in scleral form and structure play a role in the development of experimental glaucoma in mice, and potentially in human glaucoma.

Keywords: sclera, mouse, collagen, X-ray scattering, glaucoma

The sclera is the principal load-bearing structure of the eye, constituting approximately 85% of the surface area of the ocular tunic in humans. The mechanical response of the sclera to intraocular pressure (IOP) is of interest in the study of glaucoma pathogenesis since, together with the cornea, the scleral connective tissues are largely responsible for transmission of IOP-derived stresses to the optic nerve head (ONH)[1,2]— a principal site of glaucomatous retinal ganglion cell (RGC) damage.[3,4]

Approximately 90% of the scleral dry weight is accounted for by type I collagen, which forms a layered, fibrous stroma interspersed with smaller amounts of other collagens, elastic fibers, and proteoglycans and populated by fibroblasts.[5] The diameter and organization of collagen fibrils are significant determinants of scleral biomechanical properties,[6] and there is evidence for their modification in both human[7–9] and experimental[9,10] glaucoma. However, it is unclear if these observations represent baseline differences potentially linked to glaucoma susceptibility, or adaptive changes in response to elevated IOP/disease, or a combination.

The mouse eye is susceptible to induced glaucoma via a number of experimental routes.[10–15] Despite differences in ONH connective tissue architecture and vasculature, mouse and primate eyes share a common site of glaucoma injury and similarly selective pattern of RGC death in response to chronic IOP elevation.[10,13,15] In the absence of significant laminar connective tissues, astrocytes in the mouse ONH appear to simulate the structure of the collagenous laminar beams in primate eyes, providing a physical link by which scleral wall tension could transfer to ONH axons and capillaries.[16] Furthermore, the molecular composition of mouse sclera closely resembles that of humans.[17] Recently, dynamic changes in scleral structure were reported in response to chronic IOP elevation in a bead injection mouse model of glaucoma.[10] These included changes in fibril diameter, scleral thickness, and number of lamellae, along with qualitative evidence of lamellar reorientation. The aim of the present study was to provide a spatial, quantitative assessment of changes in collagen fibril organization in the mouse posterior sclera in response to chronic, bead-induced experimental glaucoma.

METHODS

Animal Details and Anesthesia

All animals were treated in accordance with the ARVO Statement for the Use of Animals in Ophthalmic and Vision Research, using protocols approved and monitored by the
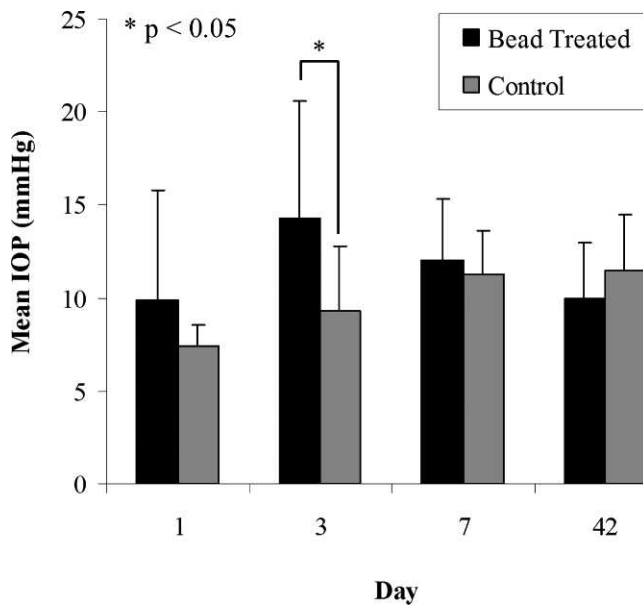
FIGURE 1. IOP readings for control and bead-treated mouse eyes as a function of post-treatment day. Values shown are mean of 12 specimens. *Error bars*: standard deviation.

Johns Hopkins University School of Medicine Animal Care and Use Committee. Twelve CD1 albino mice, aged 9 months, were obtained from Charles River Laboratories (Wilmington, MA, USA). For bead injection and baseline IOP readings, mice received anesthesia with topical application of 0.5% proparacaine hydrochloride eye drops (Akorn, Inc., Buffalo Grove, IL, USA) and additional intraperitoneal injection of 50 mg/kg ketamine, 10 mg/kg xylazine, and 2 mg/kg acepromazine. For follow-up IOP measurements, mice were anesthetized via isoflurane inhalation (2.5% in oxygen) using an RC^2 Rodent Circuit Controller (VetEquip, Inc., Pleasanton, CA, USA).

Bead Injection Protocol

Experimental glaucoma was induced in one eye of each animal via bead injection, while the untreated fellow eye served as a normal control. The bead injection protocol has been described in detail previously.[10,18] In brief, while holding the conjunctiva with forceps to stabilize the eye, a 50-μm-diameter tip glass cannula attached to a Hamilton syringe (Hamilton Company, Reno, NV, USA) was used to deliver the bead and viscoelastic solution into the anterior chamber via intracameral injection. The injected material consisted of 2 μL 6-μm-diameter and 2 μL 1-μm-diameter sterile microbeads (Polybead Microspheres; Polysciences, Inc., Warrington, PA, USA) followed by 1 μL 10 mg/mL sodium hyaluronate viscoelastic solution (Healon; Advanced Medical Optics, Inc., Santa Ana, CA, USA).

IOP Measurement

All IOP measurements were made using the TonoLab tonometer (TioLat, Inc., Helsinki, Finland), recording the mean of six readings with optimal variability grade. Baseline IOP was measured prior to injection, with follow-up readings taken at 10 minutes (to check for extreme pressure elevation), 1 day, 3 days, 1 week, and 6 weeks post treatment. Intraocular pressure data are shown in Figures 1 and 2. Mean IOP increase at peak was calculated to be 16.3 (±4.8) mm Hg. The cumulative difference between the IOP-elevated eye and fellow eye was
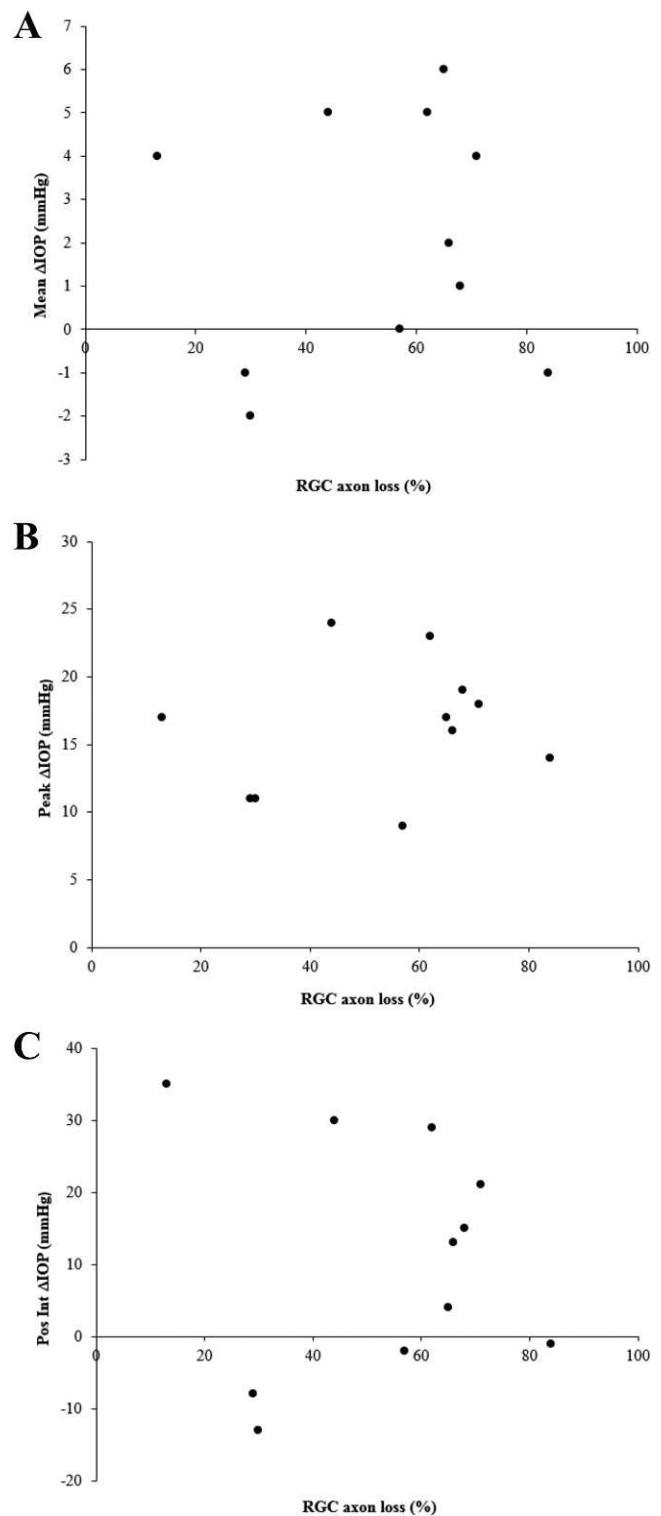

FIGURE 2. IOP versus RGC axon loss data per animal for 11 out of 12 of the mice used in this study (RGC loss was not recorded for one animal). IOP difference between treated and control eye is expressed as (**A**) mean, (**B**) peak, and (**C**) positive integral value over the 6-week treatment period. Axon loss is expressed as percent loss in treated eye compared to pooled control.

calculated as the positive integral IOP, summarizing the area under the IOP versus time curve for each eye, and totaling the area during which treated eye exceeded control eye in mm Hg—days.
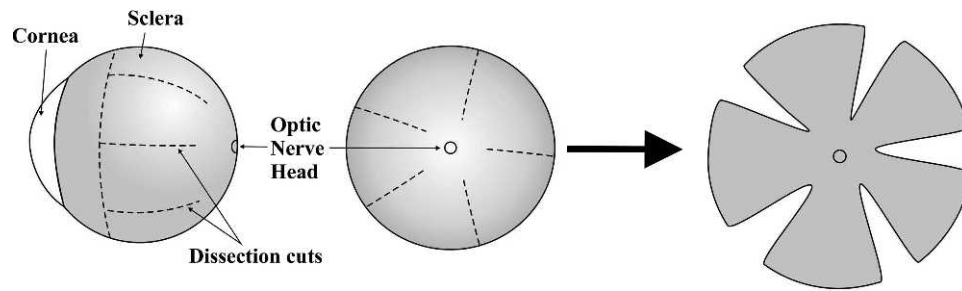
Figure 3. Dissection protocol for preparation of mouse posterior scleral flat mounts for X-ray analysis.

RGC Assessment

Six weeks after injection, animals were euthanized under general intraperitoneal anesthesia followed by exsanguination and 10-minute intracardial perfusion with 4% paraformaldehyde in 0.1 M sodium phosphate buffer (pH 7.2). To assess RGC damage, axon loss in optic nerve cross sections was estimated by a quantitative sampling technique based on previously validated methods.[19,20] After perfusion fixation and enucleation of the globes, the optic nerves were excised and placed in 1% osmium, dehydrated in ascending alcohol concentrations, and then removed to 1% uranyl acetate in 100% ethanol for 1 hour. Optic nerves were embedded in epoxy resin mixture at 60°C for 48 hours. One-micron-thick cross sections of the optic nerve were cut and digital images of the nerves taken at low power to measure each optic nerve area. High-power images were then taken (100×, oil immersion objective) using a Cool Snap camera (Photometrics, Tucson, AZ, USA) and Metamorph Image Analysis software (Molecular Devices, Downington, PA, USA). For each nerve, five 40- × 40-µm fields were sampled, representing 9% of the total nerve area. Masked observers edited nonaxonal elements from each image, generating an axon density from the software. The average axon density/mm^2 was multiplied by the individual nerve area to estimate the axon number. Values in treated eyes were compared to the mean axon number in pooled, untreated contralateral controls to yield percent axon loss. Axon loss data are shown in Figure 2.

X-Ray Scattering—Tissue Preparation

Immediately after excision of the optic nerve, the perfused enucleated globes were returned to 4% paraformaldehyde for scleral X-ray studies. Full-thickness posterior scleral flat mounts were prepared from each mouse eye using a protocol adapted from Pijanka et al.[21] for the X-ray analysis of human scleral collagen. Firstly, any remnant fat, muscle, episcleral, or optic nerve tissues were gently removed. The cornea and anterior sclera were then excised via an incision just forward of the equator using microdissection scissors, and the lens, retina, and choroid were subsequently removed. Flattening of the posterior scleral cup was achieved by making five meridional incisions, beginning at the equator and ending in the midposterior sclera approximately 1 mm from the center of the ONH, leaving the peripapillary sclera intact (Fig. 3). Following dissection, the specimens were returned to 4% paraformaldehyde until the time of X-ray examination.

X-Ray Scattering—Data Collection

Scleral collagen fibril organization was assessed using a wide-angle X-ray scattering (WAXS) method that was previously developed and applied by our lab to characterize human sclera[8,21] and that allows quantification of preferential collagen fibril orientation and content as average measures of the full, intact scleral thickness. Wide-angle X-ray scattering experiments were performed on Beamline I02 at the Diamond Light Source UK synchrotron (Didcot, UK). For examination, specimens were wrapped in polyvinylidene chloride film to prevent tissue dehydration and mounted inside Perspex (Lucite Group Ltd., Southampton, UK) chambers with Mylar (DuPont-Teijin, Middlesbrough, UK) windows. The incident X-ray beam was directed perpendicular to the surface of each flattened specimen. Wide-angle X-ray scattering patterns resulting from an X-ray exposure of 2 seconds were collected at 0.15-mm (horizontal) × 0.15-mm (vertical) intervals covering a 3- × 3-mm area centered on the ONH (Fig. 4). The WAXS patterns were recorded electronically on a Pilatus-6MF silicon pixel detector (Dectris Ltd., Baden, Switzerland) placed 250 mm behind the specimen position. Precise translation of the specimen between exposures was achieved using a motorized x–y stage interfaced with the X-ray camera shutter. The focused X-ray beam had a wavelength of 0.09795 nm and measured 0.1 mm in the horizontal and vertical dimensions.

X-Ray Scattering—Data Analysis

The scleral WAXS pattern features an equatorial (i.e., perpendicular to the fibril axis) X-ray reflection from the regular ∼1.6-nm spacing of the constituent collagen molecules aligned near axially within the fibrils (Fig. 5A). Analysis of the angular distribution of intensity around this reflection provides quantification of the collagen fibril orientation distribution within the scleral plane, as an average measure of the tissue volume traversed by the X-ray beam.[8,21] In the current study, we adapted this method for mouse sclera to obtain three collagen structure parameters for every sampled point in the tissue: the main directions and associated angular distributions of preferentially orientated collagen fibrils; the total fibrillar collagen content (irrespective of orientation); and the degree of collagen anisotropy (amount of preferentially aligned collagen as a proportion of the total fibrillar collagen content).

For every specimen, a WAXS pattern recorded from just outside the tissue was subtracted pixel by pixel from each WAXS pattern recorded from the tissue using Fit2D X-ray analysis software (A.P. Hammersley, ESRF, Grenoble, France). This removed diffuse background scatter from the Mylar specimen cell windows and polyvinylidene chloride wrapping film, and also corrected any spatial nonuniformity in the detector response. Further background subtraction was then applied to remove scatter from scleral components other than fibrous collagen using a bespoke Visual Basic for Applications (VBA) macro running in Excel (Microsoft, Reading, UK), a detailed description of which can be found in a previous publication.[22] In brief, 256 equally spaced radial profiles from pattern center to beyond the collagen signal were generated,
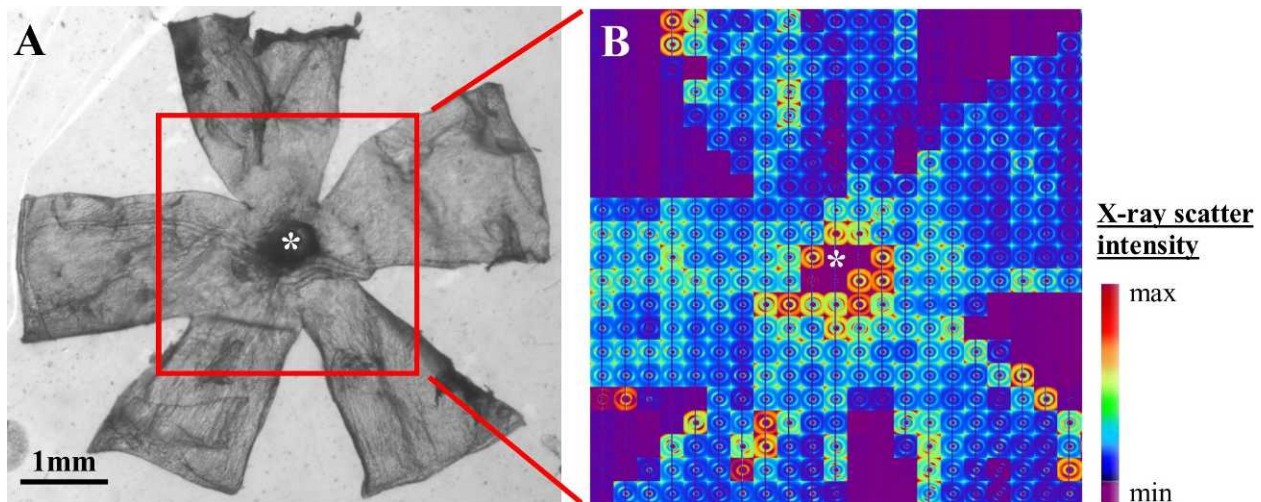
FIGURE 4. (**A**) Light microscope image of a mouse scleral flat mount prior to WAXS analysis. The area of the specimen scanned with X-rays is shown bounded by the *red rectangle*, and the ONH center is marked by an *asterisk*. (**B**) Montage of WAXS patterns recorded from the specimen.

and a unique power-law background function was independently fitted to, and subtracted from, each (Fig. 5B). The isolated collagen scatter peak for each of the 256 angular directions was subsequently normalized against fluctuations in X-ray beam current and exposure time and radially integrated, and the resulting values were extracted to angular bins using a combination of Optimas 6.5 (Media Cybernetics, Inc., Marlow, UK) image analysis software and Excel. The resulting angular intensity profile (Fig. 5C) was divided into isotropic and anisotropic scatter components, and the latter were plotted in polar vector coordinates using Statistica 7 (StatSoft Ltd., Bedford, UK), incorporating a $\pi/2$ angular shift to account for equatorial scatter. Every sampled point in the mouse sclera could thereby be represented by a polar vector plot (Fig. 5D), in which the vector length gave the relative number of fibrils preferentially aligned in the vector direction. Individual plots were assimilated using Excel into montages showing the direction and associated angular distribution of preferential fibril orientations across the specimens; and, in addition, averaged maps of the 1.5-mm-diameter area centered on the ONH were produced for the treatment and control groups.

In order to quantitatively compare preferential collagen orientation between treatment and control groups, correlation analysis was performed on the corresponding averaged fibril orientation distribution functions. This analysis compared the shape of the polar vector plots, and hence the alignment of the collagen, by comparison of the relative X-ray intensity (and hence relative fibril number) at each angle. The method compared only the shape of the plots (relating to the preferred fibril directions and associated dispersion) while ignoring the overall size of each plot (related to the overall amount of collagen). Each correlation yielded a coefficient value between -1 and $+1$ that revealed how similar the preferred directions were between them, with a more positive value indicating similarity and a more negative value indicating difference. For each sampled point, the treatment group average was correlated against the control group average using the correlation function shown in Equation 1, where T_j and C_j represent the corresponding aligned scatter (I_a) group averages for the treatment and control groups, respectively, within each angular bin, j. The results were used to produce a spatial correlation map in MATLAB software (The MathWorks, Inc., Natick, MA, USA).

$$Correl(T, C) = \frac{\sum_{j=1}^{256}(T_j - \bar{T_j})(C_j - \bar{C_j})}{\sqrt{\left(\sum(T_j - \bar{T_j})^2 \sum(C_j - \bar{C_j})^2\right)}} \quad (1)$$

Spatial distribution maps of fibrillar collagen content at each sampled point were produced in MATLAB using the integrated values of the total scatter intensity distributions (including both aligned and isotropic components, Fig. 5C) for each sampled location on the tissue, according to Equation 2, following the approach used previously in corneal WAXS studies.[22]

$$Total\_Collagen = \int_0^{2\pi}(I_a + I_i)d\phi \quad (2)$$

Corresponding maps of collagen anisotropy were also produced in MATLAB, by dividing the integrated value of the aligned scatter distribution by the corresponding integrated value of the total scatter distribution (Fig. 5C), according to Equation 3, as described previously.[8]

$$Anisotropy = \frac{\int_0^{2\pi} I_a d\phi}{\int_0^{2\pi}(I_a + I_i)d\phi} \quad (3)$$

The collagen distribution maps were subject to a cubic spline smoothing algorithm, applied by MATLAB, to aid visual interpretation of the spatial trends of the data. This process induces a constant minimum artifact at the map edges that is due to the algorithm interpolating between finite values within the tissue and zero values outside. However, calculation of all numerical regional average values reported in this paper, along with all statistical analyses, were done using unsmoothed data and were thus not subject to the edge artifact.

Statistical Analysis

Collagen anisotropy and content, by scleral region and sector, were compared between treatment and control groups. The 1.5-mm-diameter area centered on the ONH was considered in the statistical analysis, thus excluding data near the tissue cuts. Data points within a 0.5-mm radius of the ONH center were
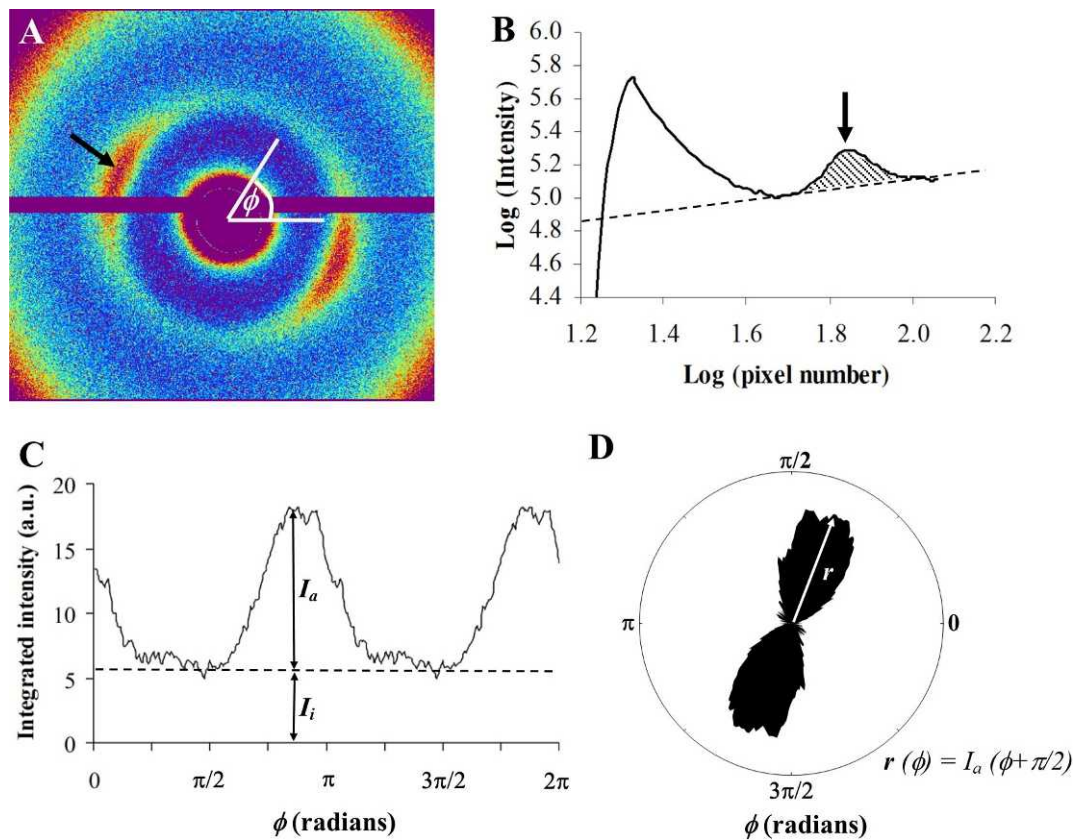
FIGURE 5. **(A)** WAXS pattern from the peripapillary region of mouse sclera. The spread of X-ray scatter intensity as a function of azimuth angle, φ, around the collagen intermolecular reflection (*arrow*) can be analyzed to obtain the fibril orientation distribution. The two-lobed appearance of the current pattern is indicative of locally uniaxial preferential fibril alignment at this point in the tissue. **(B)** Power-law background function (*broken line*) fitted to a radial profile (*solid line*) through pattern shown in **(A)**. For each pattern, 256 individual such background functions were fitted and subtracted along 256 equally spaced radial directions, enabling the collagen signal to be isolated and extracted in two dimensions. *Arrow*: collagen signal peak. **(C)** Angular X-ray scatter intensity profile of pattern shown in **(A)**. The scatter intensity may be separated into that arising from isotropically arranged collagen fibrils, I_i, and that arising from preferentially aligned fibrils, I_a. **(D)** Aligned collagen scatter displayed as a polar vector plot, whose shape reveals the collagen anisotropy. The length of vector, $r(\varphi)$, is proportional to the relative number of fibrils preferentially aligned at angle $\varphi + \pi/2$.

designated the peripapillary sclera, while data points lying between 0.5 and 0.75 mm from the ONH center were considered midposterior sclera. The two defined regions were then further subdivided into equal inferior, superior, temporal, and nasal sectors (Fig. 6). Mean anisotropy (expressed as percent aligned collagen) and collagen content (relative scatter from fibrillar collagen in AU) per region (average) and sector were then calculated for each specimen in MATLAB and statistically compared between groups using two-tailed paired *t*-tests.

The effects of IOP difference (at each postinjection measurement time point) between treated and untreated eyes, positive ΔIOP integral, and percent axon loss in treated eyes compared to pooled controls, on anisotropy, were analyzed using linear regression models in SAS 9.2 (SAS Institute, Cary, NC, USA). Residuals from these models were normally distributed. The effects of the same predictor variables on total collagen were analyzed using Spearman correlation coefficients, as the residuals from these linear models were found to be non-normally distributed. The effect of region on anisotropy and total collagen was analyzed using GEE (Generalized Estimating Equation) models, accounting for the correlation between measurements taken from peripapillary and midposterior regions of an individual mouse eye. Residuals from the GEE models were normally distributed.
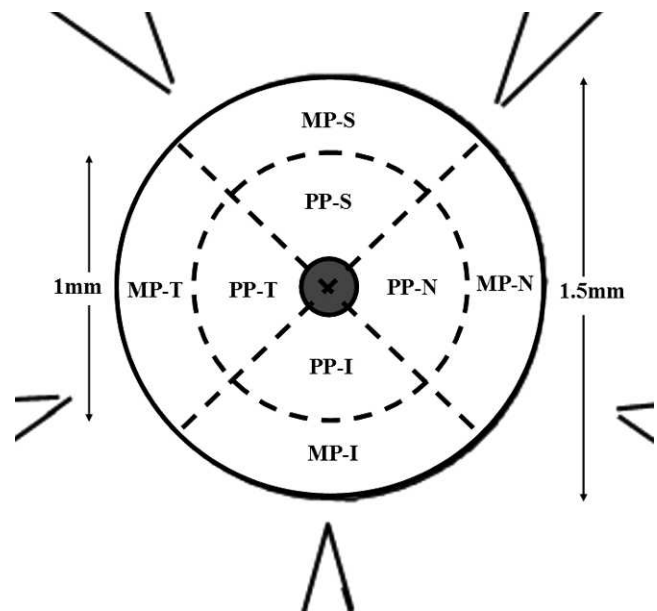

FIGURE 6. Defined regions and sectors for statistical analysis of collagen anisotropy and content. MP, midposterior sclera; PP, peripapillary sclera; S, superior; N, nasal; I, inferior; T, temporal. *Grayed area* denotes ONH.
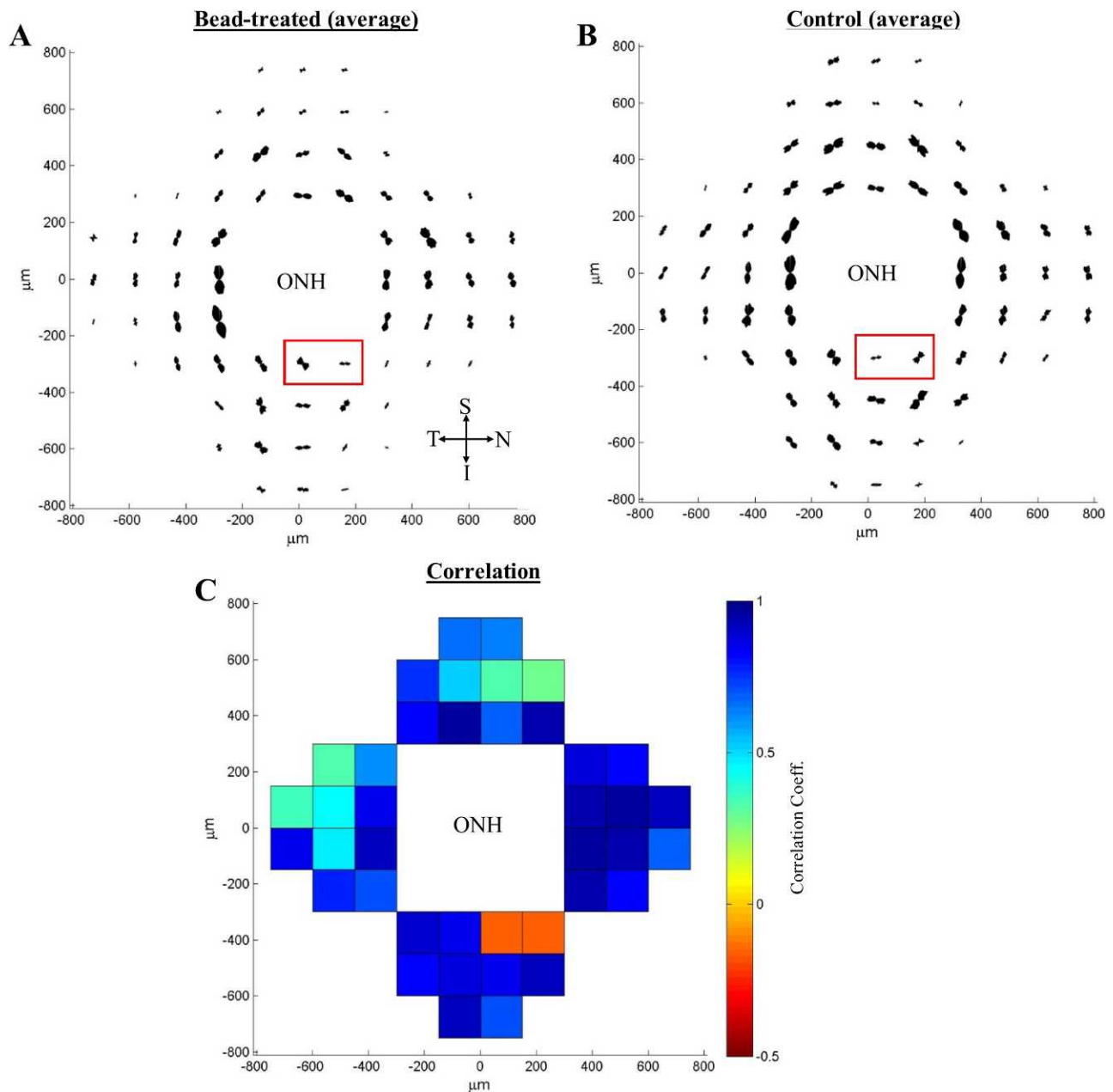
FIGURE 7. Polar vector maps of preferentially aligned collagen fibril orientation in the posterior sclera of (**A**) bead-treated and (**B**) control mouse eyes. Each map is an average of 12 specimens. The peripapillary scleral area lining the ONH canal on the inferior side, bounded by the *red rectangle*, was the only location to display major differences in dominant fibril orientation. (**C**) Correlation map comparing the shape of the vector plots point for point between (**A**) and (**B**). The superior (S), nasal (N), inferior (I), and temporal (T) directions are indicated. Negative correlation values, corresponding to the *red rectangular area* in (**A**) and (**B**), provide confirmation of the visible differences in collagen orientation between control and treatment groups in the inferior peripapillary sclera.

RESULTS

Polar vector maps of preferential collagen fibril orientation across bead-treated scleras and contralateral controls (averages of 12 specimens) are shown in Figures 7A and 7B, respectively. For both groups, a generally circumferential preferential orientation of collagen was evident, which was more pronounced with increasing proximity to the ONH. The exception was the inferior sector adjacent to the canal edge, where significant disturbance to the circumferential arrangement was observed. The inferior peripapillary area in the mouse is known to have two or three channels for major retinal blood vessels. A point-for-point correlation of the collagen fibril distributions between groups is presented alongside the averaged vector maps in Figure 7C. This confirmed the overall similarity in collagen fibril arrangements between the treatment and control groups, as indicated by the high positive correlation coefficients obtained, with the most closely correlated fibril distributions generally located proximal to the ONH. The inferior sector again represented the major exception to the general pattern, with a marked difference in fibril orientation, as disclosed by the vector directions (Figs. 7A, 7B) and resulting negative correlation coefficients (Fig. 7C), evident in the inferior peripapillary sclera immediately adjacent to the ONH.
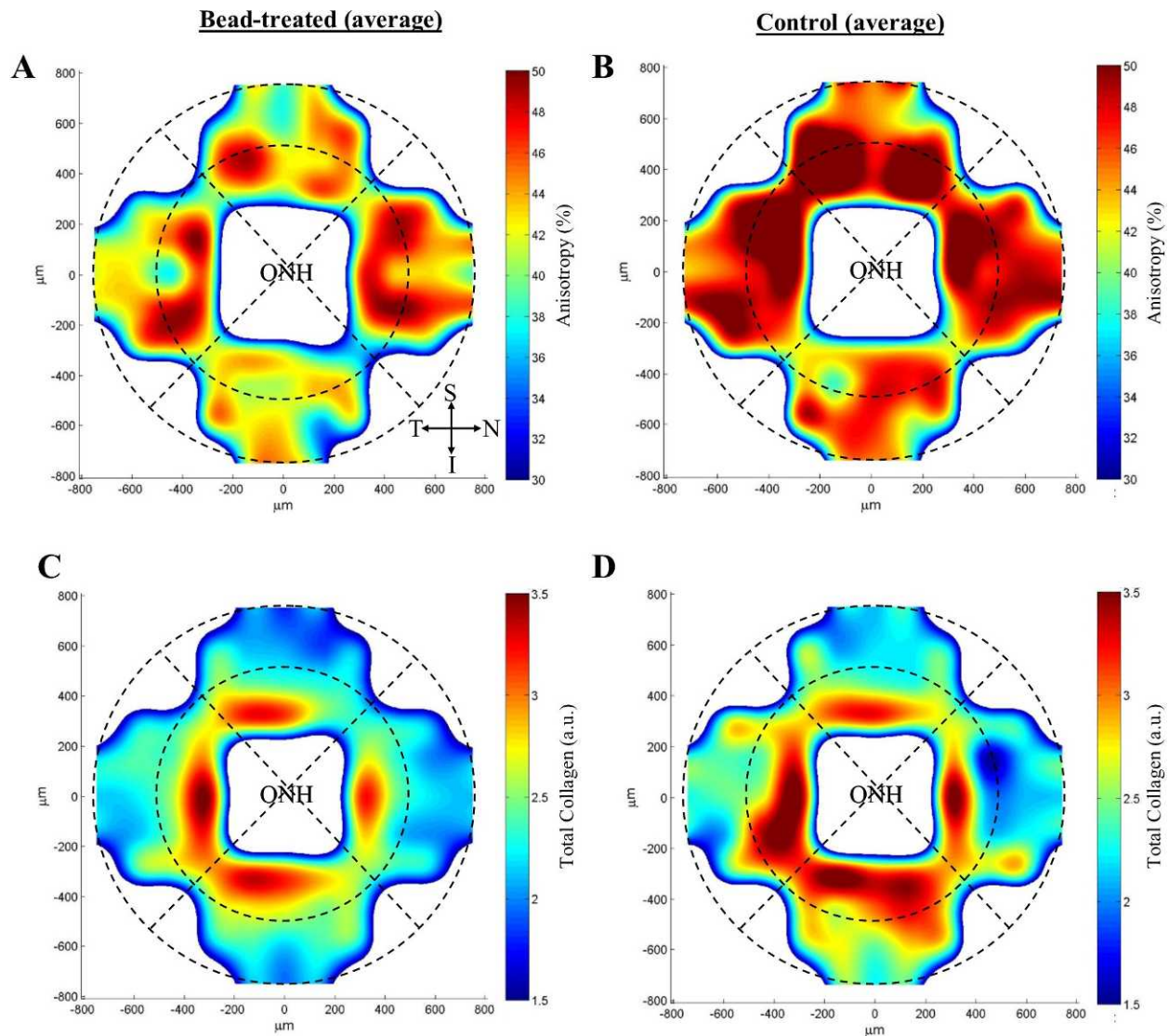
FIGURE 8. Contour maps of (**A**, **B**) collagen fibril anistropy and (**C**, **D**) total fibrillar collagen content in the posterior sclera of bead-treated and control mouse eyes. Each map is an average of 12 specimens. The peripapillary and midposterior tissue regions are delineated by *broken lines*. The superior (S), nasal (N), inferior (I), and temporal (T) directions are indicated. The map data have been smoothed using cubic spline interpolation.

Contour maps of collagen anisotropy, expressed as percent aligned collagen, for bead-treated scleras and contralateral controls (average of 12 specimens) are shown in Figures 8A and 8B, respectively. Collagen anisotropy varied markedly with circumferential location around the ONH for both groups and was, in general, higher in the peripapillary sclera (Treated: $43 \pm 6\%$; Control: $47 \pm 3\%$) compared to the midposterior sclera (Treated: $39 \pm 3\%$; Control: $43 \pm 4\%$). Univariate analysis confirmed region as a significant predictor of anisotropy ($P \leq 0.001$) (Table 1). Mean anisotropy was lower in all scleral areas in bead-treated mice (Figs. 8A, 8B; Table 2). Region- and sector-wise statistical comparison between groups indicated a significant ($P < 0.05$) reduction in mean percent aligned collagen in bead-treated compared to control mice in the superior sector of the peripapillary sclera and midposterior sclera and in the peripapillary sclera as a whole (Table 2).

Contour maps of fibrillar collagen content, expressed as relative collagen X-ray scatter (AU), for bead-treated scleras and contralateral controls (average of 12 specimens) are shown in Figures 8C and 8D, respectively. Similar to the pattern of anisotropy, collagen content was higher in the peripapillary

sclera (Treated: 2.7 ± 0.4; Control: 2.6 ± 0.6) compared to the midposterior sclera (Treated: 2.0 ± 0.3; Control: 2.1 ± 0.5), but varied less markedly with circumferential position around the ONH. Univariate analysis confirmed region as a significant predictor of collagen content ($P < 0.0001$) (Table 1). Mean collagen content was marginally reduced in all sectors of the peripapillary sclera and marginally elevated in all sectors of the midposterior sclera in bead-treated mice compared to controls (Figs. 8C, 8D; Table 2). However, in a region- and sector-wise statistical comparison between groups, all differences were outside the significance threshold ($P > 0.05$) (Table 2).

Linear regression analysis indicated no significant correlation between collagen structure parameters (anisotropy, total collagen) and RGC loss in either treated or control eyes ($P > 0.05$). No significant correlation was found between collagen parameters and IOP difference between treated and control eyes at 1 day, 3 days, and 42 days post injection, or between collagen parameters and positive ΔIOP integral ($P > 0.05$). Peripapillary anisotropy was positively correlated with ΔIOP at 7 days in the treated eye ($P < 0.05$) (Table 1).

TABLE 1. Summary of Statistically Significant ($P < 0.05$) Results From Univariate Regression Analysis

Outcome Variable	Predictor Variable	Direction of Association	*P* Value
Anisotropy, peripapillary	ΔIOP at 7 d	Positive	0.02
Anisotropy, treated eye	Region	Peripapillary > midposterior	<0.0001
Anisotropy, control eye	Region	Peripapillary > midposterior	0.001
Total collagen, treated eye	Region	Peripapillary > midposterior	<0.0001
Total collagen, control eye	Region	Peripapillary > midposterior	<0.0001

DISCUSSION

This paper presents a quantitative, spatial assessment of collagen fibril organization in the posterior sclera of mice with bead-induced chronic elevated IOP and confirmed RGC axon loss, and compares the findings with corresponding data from contralateral untreated controls. The peripapillary sclera, and to a lesser extent the midposterior tissue, of both normal and bead-treated mouse eyes were found to exhibit a largely circumferential alignment of fibrillar collagen with respect to the ONH canal. This feature has been well documented previously in humans,[8,23-25] mice,[10] and other animals,[26-28] and is predicted from numerical simulations to limit canal expansion in response to changes in IOP.[25,29,30] Thus, any disruption or variation in uniformity in this structure may presumably have implications for the stresses experienced by ONH axons as IOP fluctuates, a concept that has some support from numerical model predictions in human sclera. Work by Girard et al.[30] and more recently Grytz et al.[31] supports the notion that the anisotropic fibril architecture of the posterior sclera, and in particular the circumferential peripapillary collagen, is mechanically adapted for optimal load-bearing conditions. Moreover, a study by Coudrillier et al.[29] has shown that the biomechanical response of the ONH is critically sensitive to regional alterations in collagen anisotropy in the surrounding peripapillary sclera. The results of the current

study indicated that the circumferential alignment of collagen in the peripapillary sclera was less uniform on the inferior side of the ONH canal in CD1 control mouse eyes (Fig. 7B). This result was expected due to the inferior entry of the major retinal blood vessel canals in the murine eye,[32] and is compatible with recent second harmonic imaging of peripapillary scleral collagen in normal CD1 mice.[10] Moreover, correlation analysis of collagen vector plots in the present work (Fig. 7C) revealed further perturbation of the preferred scleral collagen alignment lining the inferior ONH canal in bead-treated eyes. This observation contrasted markedly with the situation in the remainder of the peripapillary sclera, where collagen orientations were strongly positively correlated with controls (Fig. 7C). It seems likely that in the mouse eye, the otherwise highly stable arrangement of circumferential peripapillary collagen is locally weakened on the inferior side by the nearby presence of the vessel entries, possibly rendering it more labile under fluctuating IOP. As found previously[33] and herein (Fig. 1), IOP elevation in the mouse bead model is fluctuating, with IOP receding after approximately 3 weeks to approximately normal levels. It is likely that the transient response is a consequence of the rapid increase in eye size induced by the initial IOP elevation,[18,33,34] which the current and previous[10,35] work suggests is linked to collagen remodeling. In human glaucoma, both the height of IOP[36] and its fluctuation[37] contribute to RGC damage. Thus, some variability in IOP during the course of the current experiments may more closely simulate human disease.

A notable finding of the current study was the significant reduction in anisotropy in the peripapillary region of bead-treated compared to control mouse scleras (Figs. 8A, 8B; Table 2). This observation agrees well with previous qualitative imaging of scleral collagen in glaucomatous CD1 mice, in which bead-induced chronic IOP elevation resulted in a more random arrangement of peripapillary fibril bundles,[10] and is consistent with prior inflation studies of CD1 experimental glaucoma models. A decrease in the degree of fibril alignment indicates a more random, isotropic structure and a more isotropic mechanical behavior. Inflation studies of the CD1 bead injection model[38] showed that the averaged ratio of meridional to circumferential strains at 30 mm Hg was smaller for glaucoma compared to normal eyes, which indicates a more isotropic mechanical behavior, assuming that there was no change to the principal curvatures (shape) of the posterior sclera. Differences in the degree of alignment of posterior scleral collagen have also been reported between non-glaucoma and glaucoma human eyes,[7,8] but it is not known whether these precede, accompany, or follow disease progression. While studies in both monkeys[39] and mice[34] have indicated that a combination of baseline differences and dynamic changes in scleral structure likely contributes to injury susceptibility in experimental glaucoma, there is evidence to suggest that, in the mouse at least, the sclera's dynamic response to IOP elevation may play the more influential role.[10,18,38] The results of the current study support this view, and further suggest that significant changes

TABLE 2. Comparison of Mean Collagen Fibril Anisotropy and Content by Scleral Region and Sector Between Bead-Treated and Control Mouse Scleras ($n = 12$)

Region/Sector	Group	Anisotropy, % (SD)	Collagen Content, AU (SD)
PP inferior	Treated	40 (±7)	2.8 (±0.5)
	Control	43 (±7)	2.7 (±0.8)
PP superior	Treated	43 (±8)*	2.6 (±0.4)
	Control	49 (±6)*	2.4 (±0.6)
PP temporal	Treated	45 (±7)	2.8 (±0.5)
	Control	49 (±6)	2.7 (±0.8)
PP nasal	Treated	44 (±10)	2.7 (±0.4)
	Control	47 (±5)	2.5 (±0.7)
PP all	Treated	43 (±6)*	2.7 (±0.4)
	Control	47 (±3)*	2.6 (±0.6)
MP inferior	Treated	39 (±4)	2.1 (±0.3)
	Control	42 (±5)	2.1 (±0.1)
MP superior	Treated	39 (±4)*	1.9 (±0.2)
	Control	43 (±4)*	2.0 (±0.5)
MP temporal	Treated	39 (±4)	2.0 (±0.3)
	Control	43 (±4)	2.1 (±0.6)
MP nasal	Treated	40 (±6)	2.0 (±0.2)
	Control	43 (±5)	2.1 (±0.5)
MP all	Treated	39 (±4)	2.0 (±0.3)
	Control	43 (±4)	2.1 (±0.5)

PP, peripapillary sclera; MP, midposterior sclera.
* Significant difference ($P < 0.05$).

in collagen anisotropy may impact the course of disease progression in murine glaucoma. In contrast to the situation for collagen anisotropy, the present study indicated no significant differences in total fibrillar collagen content between bead-treated and control eyes. Previous work using the same bead injection mouse model reported a concurrent increase in scleral thickness/number of lamellae and reduction in average collagen fibril diameter in glaucomatous CD1 mouse eyes.[10] These changes would tend to have opposing effects on the net amount of collagen encountered by the X-ray beam in the current work and are thus generally compatible with the present findings, possibly suggesting a homeostatic response.

Mechanistic insight into what may be driving the changes in scleral collagen organization in murine glaucoma, as disclosed herein and previously, awaits further investigation. However, prior work has pointed to the potential importance of the cellular IOP response in scleral matrix remodeling. Human scleral fibroblasts are known to be susceptible to mechanotransduction in the physiological pressure range,[40] while scleral myofibroblast activity has been shown to be upregulated in both experimental glaucoma[35] and myopia[41] animal models. In the mouse, cell transition to myofibroblast is dramatic and rapid, occurring over a few days following bead injection,[35] and is accompanied by axial eye elongation of up to 10% during the following 1 to 2 weeks.[8,33,34] Notably, it was recently reported that the number and volume of cellular lamellae are increased in the peripapillary sclera of CD1 mice following chronic pressure elevation.[10]

Although the current work indicated a positive correlation between anisotropy and IOP difference at 7 days in the treated eye (Table 1), this finding was not consistent across the remaining IOP predictive variables including, notably, the cumulative IOP integral, which accounts for the whole treatment period. To establish such a relation statistically would require a larger sample size than used in the current study. An a priori sample size calculation for a single predictor regression model estimates that, even with the most favorable input parameter conventions (largest anticipated effect size [$f^2 = 0.35$], lowest desired statistical power [0.80], lowest probability level [$P < 0.05$]), a minimum sample size of 25 animals would be required to find a significant correlation between IOP and RGC loss/collagen anisotropy. Indeed, previous studies by our lab and others, using considerably more mice than in the current investigation, have already established a statistical link between IOP elevation and RGC loss in the same experimental model. This work has demonstrated unequivocally that the mouse bead model leads directly and consistently to RGC death.[10,14,18,33,34,42–47] Moreover, the well-characterized axial enlargement of the mouse eye in response to bead treatment is strongly indicative of a direct relationship between IOP elevation and scleral reorganization,[10,18,33,34,47] and is also a characteristic of young human eyes with glaucoma. Sappington et al.[14] first showed a direct correlation between bead-induced IOP elevation and RGC loss in rats and mice. Subsequent studies of over 1000 mice using this model in our lab showed that IOP elevation directly causes axial elongation and RGC death. Cone et al.[34] demonstrated that bead and viscoelastic injection produced IOP elevation in 94.1% of eyes ($n = 112/119$). By 6 to 12 weeks, injected eyes were 10.8% longer. Retinal ganglion cell layer loss and axon loss were significantly related by linear regression. In a subsequent study with 669 mice,[18] the protocol used in the present study was described and shown to produce consistent and significant IOP elevations in treated compared to control eyes, and shown to be directly related to RGC axon loss; while a recent

study in the same model[47] showed that higher IOP exposure correlates with greater RGC loss.

The relevance of the mouse bead injection glaucoma model to human disease has been demonstrated in the literature. Many other investigators have found that bead-induced IOP elevation leads to RGC dysfunction[43,44] and death[42,45]; that such bead-induced IOP elevation can be reduced by eye drop–delivered drugs used in humans; and that IOP reduction, as in human glaucoma, reduces the loss of RGC.[46] The location of axonal pathology in mice in the current model is at, and just behind, the ONH, where its morphology is identical to that in human glaucoma. Axonal transport disruption, as seen in human glaucoma, is also found in this model. Moreover, regional changes in collagen anisotropy in the mouse, as identified herein, resemble those previously reported in human glaucoma using the same X-ray technique.[8]

This study was subject to a number of limitations. As mentioned, the connective tissue and vascular organization of the lamina cribrosa differ fundamentally between the mouse and primate eye. Related to this, the pattern of vessel canal entries in the peripapillary sclera, which the current data suggest may have some bearing on the pattern of fibrillar perturbation observed as glaucoma progresses, is also very different in mice and humans. In addition, the mouse eye is some 10-fold smaller, while the time course of murine experimental glaucoma is much shorter than in the human disease. These factors should be taken into account in interpreting the results of the current work in the context of human glaucoma. The WAXS method used herein also has some inherent limitations. Firstly, as the WAXS signal is of molecular origin,[22] the helicoidal packing of the microfibrillar subunits comprising the fibrils produces an angular broadening of the WAXS diffraction peaks, leading to a general underestimation in the degree of fibril anisotropy. In sclera the microfibrillar tilt angle with respect to the fibrillar axis is relatively small ($\sim 5°$),[48] and we therefore predict our underestimation of fibril anisotropy to be accordingly minor. Secondly, dissection and flattening of the mouse globes may have released some of the residual stress present within the intact tissue, potentially leading to changes in the natural collagen orientation, especially near the cut edges. However, studies in other collagenous tissues suggest that this effect tends to be more evident at the macro (organ) level and less so at the level of the collagen microstructure.[49] Moreover, our fixation of the eyes in their natural curvature (prior to dissection) will likely have further minimized any collagen reorganization upon flattening. Nevertheless, in the present study we restricted our statistical analysis to the central 1.5-mm area around the ONH to avoid inclusion of data points near the meridional cuts.

In summary, we have demonstrated that significant spatial changes in collagen fibril anisotropy occur in the posterior sclera of mice with chronic, bead-induced IOP elevation and confirmed axon loss. These results support the idea that dynamic changes in scleral form and structure may play an important role in the development of experimental glaucoma in mice, and further, demonstrate the wider potential of the mouse as a model system in which to study ocular remodeling processes. Further study of the bead injection murine glaucoma model may offer some insight into certain aspects of human glaucoma pathophysiology, with the above-mentioned caveats.

References

1. Downs JC, Roberts MD, Burgoyne CF. Mechanical environment of the optic nerve head in glaucoma. *Optom Vis Sci*. 2008;85: 425–435.

2. Sigal IA, Ethier CR. Biomechanics of the optic nerve head. *Exp Eye Res*. 2009;88:799–807.

3. Anderson DR, Hendrickson A. Effect of intraocular pressure on rapid axoplasmic transport in monkey optic nerve. *Invest Ophthalmol*. 1974;13:771–783.

4. Quigley HA, Addicks EM, Green WR, Maumenee AE. Optic nerve damage in human glaucoma. II. The site of injury and susceptibility to damage. *Arch Ophthalmol*. 1981;99:635–649.

5. Watson PG, Young RD. Scleral structure, organisation and disease. A review. *Exp Eye Res*. 2004;78:609–623.

6. Meek KM. The cornea and sclera. In: Fratzl P, ed. *Collagen: Structure and Mechanics*. New York: Springer; 2008:359–396.

7. Danford FL, Yan D, Dreier RA, Cahir TM, Girkin CA, Vande Geest JP. Differences in the region- and depth-dependent microstructural organization in normal versus glaucomatous human posterior sclerae. *Invest Ophthalmol Vis Sci*. 2013;54: 7922–7932.

8. Pijanka JK, Coudrillier B, Ziegler K, et al. Quantitative mapping of collagen fiber orientation in non-glaucoma and glaucoma posterior human sclerae. *Invest Ophthalmol Vis Sci*. 2012;53: 5258–5270.

9. Quigley HA, Dorman-Pease ME, Brown AE. Quantitative study of collagen and elastin of the optic nerve head and sclera in human and experimental monkey glaucoma. *Curr Eye Res*. 1991;10:877–888.

10. Cone-Kimball E, Nguyen C, Oglesby EN, Pease ME, Steinhart MR, Quigley HA. Scleral structural alterations associated with chronic experimental intraocular pressure elevation in mice. *Mol Vis*. 2013;19:2023–2039.

11. Aihara M, Lindsey JD, Weinreb RN. Experimental mouse ocular hypertension: establishment of the model. *Invest Ophthalmol Vis Sci*. 2003;44:4314–4320.

12. Nakazawa T, Nakazawa C, Matsubara A, et al. Tumor necrosis factor-alpha mediates oligodendrocyte death and delayed retinal ganglion cell loss in a mouse model of glaucoma. *J Neurosci*. 2006;26:12633–12641.

13. Ruiz-Ederra J, Verkman AS. Mouse model of sustained elevation in intraocular pressure produced by episcleral vein occlusion. *Exp Eye Res*. 2006;82:879–884.

14. Sappington RM, Carlson BJ, Crish SD, Calkins DJ. The microbead occlusion model: a paradigm for induced ocular hypertension in rats and mice. *Invest Ophthalmol Vis Sci*. 2010;51:207–216.

15. Fu CT, Sretavan D. Laser-induced ocular hypertension in albino CD-1 mice. *Invest Ophthalmol Vis Sci*. 2010;51:980–990.

16. Sun D, Lye-Barthel M, Masland RH, Jakobs TC. The morphology and spatial arrangement of astrocytes in the optic nerve head of the mouse. *J Comp Neurol*. 2009;516:1–19.

17. Zhou J, Rappaport EF, Tobias JW, Young TL. Differential gene expression in mouse sclera during ocular development. *Invest Ophthalmol Vis Sci*. 2006;47:1794–1802.

18. Cone FE, Steinhart MR, Oglesby EN, Kalesnykas G, Pease ME, Quigley HA. The effects of anesthesia, mouse strain and age on intraocular pressure and an improved murine model of experimental glaucoma. *Exp Eye Res*. 2012;99:27–35.

19. Levkovitch-Verbin H, Quigley HA, Martin KR, Valenta D, Baumrind LA, Pease ME. Translimbal laser photocoagulation to the trabecular meshwork as a model of glaucoma in rats. *Invest Ophthalmol Vis Sci*. 2002;43:402–410.

20. Marina N, Bull ND, Martin KR. A semiautomated targeted sampling method to assess optic nerve axonal loss in a rat model of glaucoma. *Nat Protoc*. 2010;5:1642–1651.

21. Pijanka JK, Abass A, Sorensen T, Elsheikh A, Boote C. A wide-angle X-ray fibre diffraction method for quantifying collagen orientation across large tissue areas: application to the human eyeball coat. *J Appl Crystallogr*. 2013;46:1481–1489.

22. Meek KM, Boote C. The use of x-ray scattering techniques to quantify the orientation and distribution of collagen in the corneal stroma. *Prog Retin Eye Res*. 2009;28:369–392.

23. Kokott W. Das spaltlinienbild der sklera (Ein beitrag zum funktionellen bau der sklera). *Klin Mbl Augenheilk*. 1934;92: 177–185.

24. Winkler M, Jester B, Nien-Shy C, et al. High resolution three-dimensional reconstruction of the collagenous matrix of the human optic nerve head. *Brain Res Bull*. 2010;81:339–348.

25. Grytz R, Meschke G, Jonas JB. The collagen fibril architecture in the lamina cribrosa and peripapillary sclera predicted by a computational remodeling approach. *Biomech Model Mechanobiol*. 2011;10:371–382.

26. Girard MJ, Dahlmann-Noor A, Rayapureddi S, et al. Quantitative mapping of scleral fiber orientation in normal rat eyes. *Invest Ophthalmol Vis Sci*. 2011;52:9684–9693.

27. Girard MJ, Suh JK, Bottlang M, Burgoyne CF, Downs JC. Scleral biomechanics in the aging monkey eye. *Invest Ophthalmol Vis Sci*. 2009;50:5226–5237.

28. Morrison JC, Lhernault NL, Jerdan JA, Quigley HA. Ultrastructural location of extracellular-matrix components in the optic nerve head. *Arch Ophthalmol*. 1989;107:123–129.

29. Coudrillier B, Boote C, Quigley HA, Nguyen TD. Scleral anisotropy and its effects on the mechanical response of the optic nerve head. *Biomech Model Mechanobiol*. 2013;12: 941–963.

30. Girard MJ, Downs JC, Burgoyne CF, Suh JK. Peripapillary and posterior scleral mechanics–part I: development of an anisotropic hyperelastic constitutive model. *J Biomech Eng*. 2009;131:051011.

31. Grytz R, Fazio MA, Girard MJ, et al. Material properties of the posterior human sclera. *J Mech Behav Biomed Mater*. 2014; 29:602–617.

32. Ritter MR, Aguilar E, Banin E, Scheppke L, Uusitalo-Jarvinen H, Friedlander M. Three-dimensional in vivo imaging of the mouse intraocular vasculature during development and disease. *Invest Ophthalmol Vis Sci*. 2005;46:3021–3026.

33. Steinhart MR, Cone FE, Nguyen C, et al. Mice with an induced mutation in collagen 8A2 develop larger eyes and are resistant to retinal ganglion cell damage in an experimental glaucoma model. *Mol Vis*. 2012;18:1093–1106.

34. Cone FE, Gelman SE, Son JL, Pease ME, Quigley HA. Differential susceptibility to experimental glaucoma among 3 mouse strains using bead and viscoelastic injection. *Exp Eye Res*. 2010;91:415–424.

35. Quigley HA, Cone FE. Development of diagnostic and treatment strategies for glaucoma through understanding and modification of scleral and lamina cribrosa connective tissue. *Cell Tissue Res*. 2013;353:231–244.

36. Bengtsson B, Heijl A. Diurnal IOP fluctuation: not an independent risk factor for glaucomatous visual field loss in high-risk ocular hypertension. *Graefes Arch Clin Exp Ophthalmol*. 2005;243:513–518.

37. Nouri-Mahdavi K, Hoffman D, Coleman AL, et al. Predictive factors for glaucomatous visual field progression in the Advanced Glaucoma Intervention Study. *Ophthalmology*. 2004;111:1627–1635.

38. Nguyen C, Cone FE, Nguyen TD, et al. Studies of scleral biomechanical behavior related to susceptibility for retinal ganglion cell loss in experimental mouse glaucoma. *Invest Ophthalmol Vis Sci*. 2013;54:1767–1780.

39. Burgoyne CF, Downs JC, Bellezza AJ, Suh JK, Hart RT. The optic nerve head as a biomechanical structure: a new paradigm for understanding the role of IOP-related stress and strain in the pathophysiology of glaucomatous optic nerve head damage. *Prog Retin Eye Res*. 2005;24:39–73.

40. Cui W, Bryant MR, Sweet PM, McDonnell PJ. Changes in gene expression in response to mechanical strain in human scleral fibroblasts. *Exp Eye Res*. 2004;78:275–284.

41. Phillips JR, McBrien NA. Pressure-induced changes in axial eye length of chick and tree shrew: significance of myofibroblasts in the sclera. *Invest Ophthalmol Vis Sci*. 2004;45:758–763.

42. Chen H, Wei X, Cho KS, et al. Optic neuropathy due to microbead-induced elevated intraocular pressure in the mouse. *Invest Ophthalmol Vis Sci*. 2011;52:36–44.

43. Della Santina L, Inman DM, Lupien CB, Horner PJ, Wong RO. Differential progression of structural and functional alterations in distinct retinal ganglion cell types in a mouse model of glaucoma. *J Neurosci*. 2013;33:17444–17457.

44. Frankfort BJ, Khan AK, Tse DY, et al. Elevated intraocular pressure causes inner retinal dysfunction before cell loss in a mouse model of experimental glaucoma. *Invest Ophthalmol Vis Sci*. 2013;54:762–770.

45. Ward NJ, Ho KW, Lambert WS, Weitlauf C, Calkins DJ. Absence of transient receptor potential vanilloid-1 accelerates stress-induced axonopathy in the optic projection. *J Neurosci*. 2014; 34:3161–3170.

46. Yang Q, Cho KS, Chen H, et al. Microbead-induced ocular hypertensive mouse model for screening and testing of aqueous production suppressants for glaucoma. *Invest Ophthalmol Vis Sci*. 2012;53:3733–3741.

47. Kimball FE, Nguyen C, Steinhart MR, et al. Experimental scleral cross-linking increases glaucoma damage in a mouse model. *Exp Eye Res*. In press.

48. Yamamoto S, Hashizume H, Hitomi J, et al. The subfibrillar arrangement of corneal and scleral collagen fibrils as revealed by scanning electron and atomic force microscopy. *Arch Histol Cytol*. 2000;63:127–135.

49. Lanir Y. Mechanisms of residual stress in soft tissues. *J Biomech Eng*. 2009;131:044506.